Key Points:
- The AMS of the Gonjo Basin records sedimentary fabrics overprinted by weak shortening
- The AMS of the Gonjo Basin indicates an increased strain related to shortening at ~52 Ma
- AMS with precise age constraint provides a powerful tool to date deformation phases, allowing discrimination between tectonic versus climatic influences on sediments

Anisotropy of Magnetic Susceptibility (AMS) Analysis of the Gonjo Basin as an Independent Constraint to Date Tibetan Shortening Pulses

Shihu Li[1,2] , Douwe J. J. van Hinsbergen[3] , Zhongshan Shen[1,4,5], Yani Najman[2] , Chenglong Deng[1,4,5] , and Rixiang Zhu[1,4,5]

[1]State Key Laboratory of Lithospheric Evolution, Institute of Geology and Geophysics, Chinese Academy of Sciences, Beijing, China, [2]Lancaster Environment Centre, Lancaster University, Lancaster, UK, [3]Department of Earth Sciences, Utrecht University, Utrecht, The Netherlands, [4]Institutions of Earth Science, Chinese Academy of Sciences, Beijing, China, [5]College of Earth and Planetary Sciences, University of Chinese Academy of Sciences, Beijing, China

Abstract The Tibetan Plateau accommodated major upper crustal shortening during Indian Plate oceanic and continental lithosphere subduction. Deciphering whether shortening was continuous or episodic, and how it correlates to major geodynamic changes is challenging. Here we apply anisotropy of magnetic susceptibility (AMS), a sensitive synsedimentary strain indicator, to a ~3 km thick magnetostratigraphically dated sedimentary section (69–41.5 Ma) in eastern Tibet. AMS shows "earliest deformation" fabrics from 69–52 Ma, followed by a sudden change to "pencil structure" fabrics with increasing anisotropy degree at ~52 Ma, dating a sudden increased synsedimentary shortening strain. This change coincides with enhanced sedimentation rates and synsedimentary vertical-axis rotations of the Gonjo Basin, suggesting a causal link to a marked India-Asia convergence rate deceleration. We show that AMS analysis provides a strong tool to distinguish between climatic and tectonic causes of sedimentological change and is an asset in identifying discrete tectonic pulses in intensely deformed terrane.

Plain Language Summary How the Tibetan Plateau evolved during India-Asia convergence and collision is notoriously challenging to decipher. Use of sedimentary records to date periods of tectonic activity is a popular approach, yet distinguishing between tectonic versus climate signals in sediment records can be challenging. The anisotropy of magnetic susceptibility (AMS) is an effective and sensitive technique that reveals tectonic stress fields during sedimentation and changes therein, even in weakly deformed clastic sedimentary rocks. We report a detailed record of AMS data from a ~3 km thick section of redbeds from the Gonjo Basin in eastern Tibet. Previous magnetostratigraphy dated deposition from 69 to 41.5 Ma; during this time period marked sedimentation rate increases and simultaneous vertical-axis rotations were interpreted to reflect shortening pulses. Our new AMS data indicate an increased shortening strain at ~52 Ma, demonstrating that the sedimentation rate changes are tectonic rather than climatic in origin, showing that a pulse in crustal shortening of Tibet occurred simultaneous with a marked ~52 Ma onset of deceleration of India-Asia convergence. We show that applying a suite of paleomagnetic and rock magnetic techniques, including magnetostratigraphy and sedimentation rate calculation, vertical-axis rotation analysis, and AMS analysis, provides a powerful tool to differentiate tectonic versus climatic influence on a sediment archive, allowing the precise dating of discrete deformation phases in intensely deformed regions that evolved over long periods of time.

1. Introduction

The Tibetan Plateau has undergone a long history of shortening at least since the Cretaceous (e.g., Kapp & DeCelles, 2019). Identifying its deformation history is of importance for analysis of geodynamics as well as paleoclimate. During the Plateau's long deformation history, several sharp geodynamic and climatic events occurred that are thought to be reflected in, or even caused by Tibetan shortening. For instance, the India-Asia convergence rate has undergone major changes around, for example, 70, 52, and 20 Ma (Molnar & Stock, 2009; van Hinsbergen et al., 2011) and the reflection of these events in the deformation of the upper crust in Tibet may provide novel constraints on the underlying dynamic drivers (e.g., Li
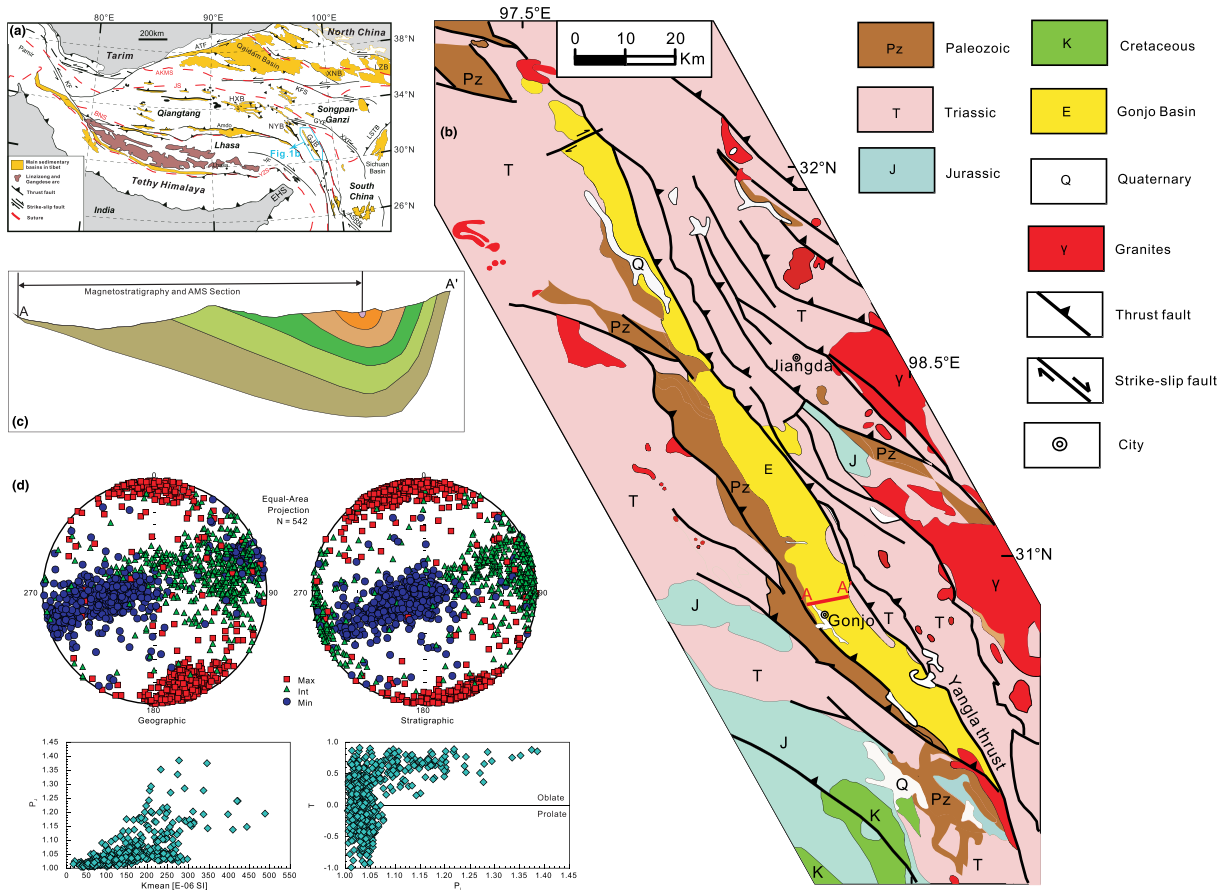
Figure 1. (a) Simplified tectonic map of the Tibetan Plateau showing the distribution of main sutures (red dashed lines), sedimentary basins (orange), and related strike-slip and thrust faults (solid black lines). The blue polygon denotes the location of the Gonjo Basin in Figure 1b. Main abbreviations: HXB: Hoh Xil Basin; NYB: Nangqian-Yushu Basin; GJB: Gonjo Basin; XNB: Xining Basin; LZB: Lanzhou Basin; EHS: Eastern Himalaya Syntaxis. (b) Geological map of the Gonjo Basin and surrounding area. (c) Cross section showing the asymmetric syncline of the Gonjo Basin along the Gonjo city Transect A-A′, modified from Studnicki-Gizbert et al. (2008). (d) All the AMS results from the Gonjo Basin, including the equal-area projections of AMS principal axes in geographic and stratigraphic coordinate, P_J-Km, and P_J-T diagrams.

et al., 2020). Meanwhile, there are marked changes in regional climate, such as aridification, that may at least in part relate to Tibetan deformation and/or uplift events (e.g., Guo et al., 2002). Establishing whether shortening in Tibet was gradual or pulsed, and if the latter, what the timing and distribution of such pulses may have been will thus be helpful in advancing our understanding of the causes and consequences the Tibetan Plateau's formation. Yet this is challenging; geological archives that hold clues to the Plateau's long-term deformation history are provided by sedimentary basins across the Tibetan Plateau, but variations in sedimentary infill may in principle be caused by climatic (e.g., Molnar, 2004) as well as tectonic influences, making such changes difficult to interpret.

Recently, a high-resolution magnetostratigraphic study (Li et al., 2020) on a ~3 km thick sedimentary section in the Gonjo Basin, located in east central Tibet (Figure 1a), revealed a 69–41.5 Ma age range for the basin. The age model suggested that the Gonjo Basin experienced two short periods of rapid sedimentation (~20 cm/kyr) at 69–64 Ma and 52–48 Ma, within longer-term periods of low sedimentation (7–8 cm/kyr) at 64–52 Ma and 48–41 Ma (Figure 2h). Because paleomagnetic declinations showed that the Gonjo Basin experienced vertical-axis rotations during these high sedimentation rate intervals but not during the low sedimentation rate intervals, the high sedimentation rate intervals were interpreted to reflect periods of enhanced tectonic deformation, which was further interpreted as crustal shortening pulses given the contractional setting in eastern Tibet (Li et al., 2020). This is interesting because the first pulse of deformation since 69 Ma is roughly synchronous with a rapid acceleration of India-Asia convergence rate, while the
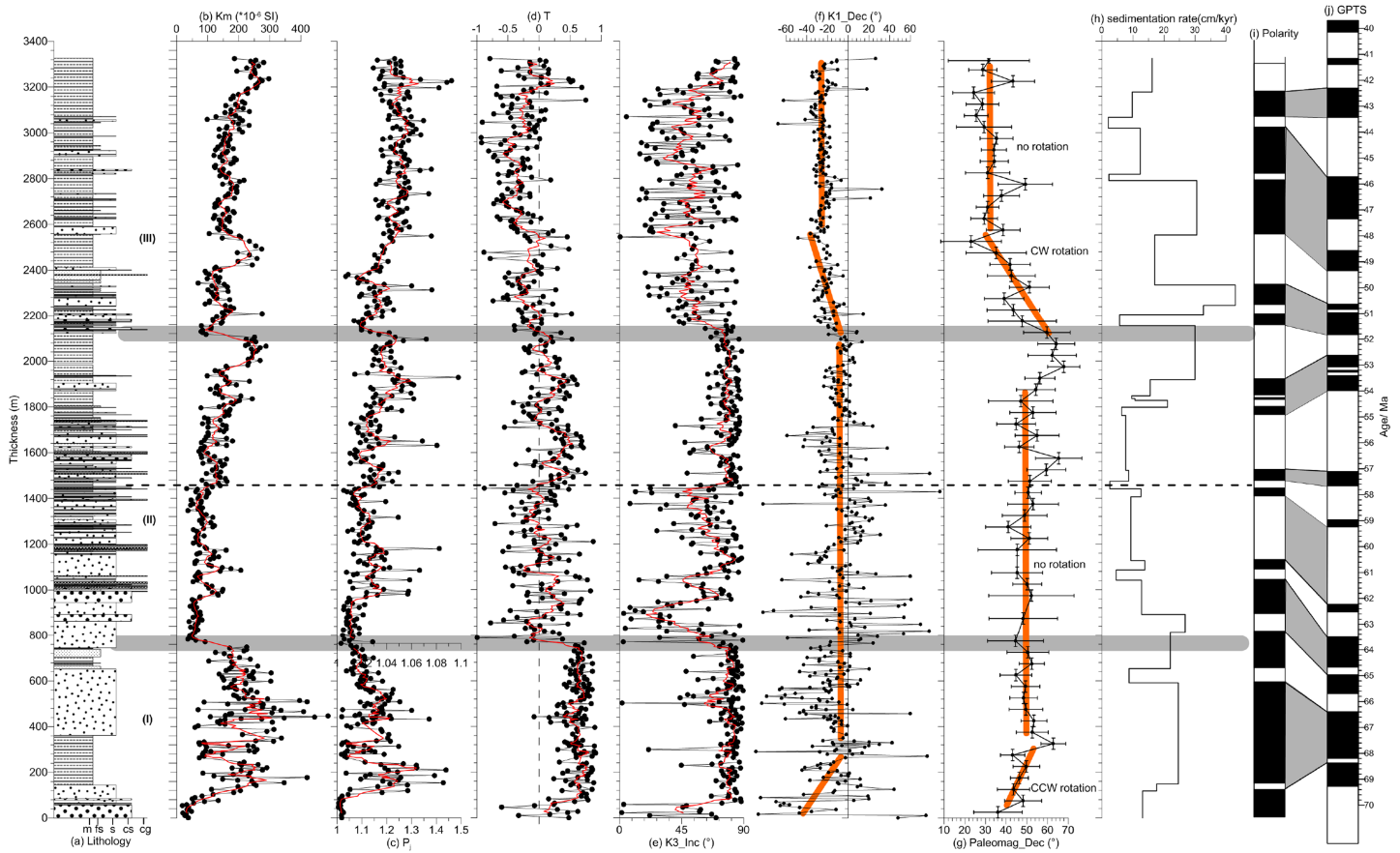
Figure 2. (a) Lithology, (b) mean susceptibility (Km), (c) corrected degree of anisotropy (P$_J$) (note the different scale of *X* axes before and after 765 m), (d) shape parameter (*T*), (e) inclinations of minimum principle axes (K3_Inc), (f) declinations of maximum principle axes (K1_Dec), (g) paleomagnetic declinations, and (h) sedimentation rate versus thickness from the Gonjo Basin. (i, j) magnetostratigraphic result of the Gonjo Basin (Li et al., 2020). m: mudstone, fs: fine sandstone, s: medium sandstone, cs: coarse sandstone, cg: conglomerate, CW: clockwise, CCW: counterclockwise. The red lines in (b)–(e) are seven points average smooth. The orange lines in (f) and (g) show the synchronous rotation patterns between paleomagnetic declinations and AMS K$_1$ declinations. The AMS parameter can be subdivided into three intervals as shown by the gray lines (see text for details). The dashed line represents the onset of India-Asia collision at 59 ± 1 Ma (Hu et al., 2015). Note that AMS parameters, sedimentation rate, and paleomagnetic declinations do not show any change at the time of India-Asia initial collision.

second pulse of deformation since 52 Ma is synchronous with a major deceleration of India-Asia convergence rate. These interpretations predict that the periods of high sedimentation rate coincide with enhanced shortening strain, which should then be recorded in the sedimentary record.

In this paper, we study the Gonjo section in detail using anisotropy of magnetic susceptibility (AMS). This is a petrofabric tool able to determine the preferred orientation of particles under an external field (e.g., gravity, wind, magnetic field, flow, and strain) during deposition and diagenesis of rocks. The AMS method has been widely employed as an easy, fast, economic, and sensitive rock strain indicator (e.g., Borradaile, 1988; Borradaile & Henry, 1997; Graham, 1954; Kissel et al., 1986) and has been widely successfully applied in sedimentary basins to detect regional deformation (e.g., Gilder et al., 2001; Gong et al., 2009; Li et al., 2014; Maffione et al., 2015; Mattei et al., 1997; Parés et al., 1999; Soto et al., 2009; Z. Tang et al., 2012; van Hinsbergen et al., 2005). In this study we apply the AMS as an independent method to constrain the timing of crustal shortening pulses and to test whether the high sedimentation rate intervals coincide with enhanced AMS fabrics.

2. Geological Setting and Methods

The Gonjo Basin (30.85°N, 98.3°E) is located in the eastern part of the Qiangtang terrane, northeast of the Eastern Himalayan Syntaxis (Figure 1a). The subsidence and structure of the Gonjo Basin was controlled by the Yangla thrust fault to the east, which carried Triassic rocks over the basin margin in the northeast (Studnicki-Gizbert et al., 2008; M. Tang et al., 2017; Figure 1b). The basin sediments are now exposed in

an asymmetric syncline (Figure 1c), where the strata in the western limb are significantly thicker and shallower than those in the eastern limb. This, together with the presence of growth strata in the eastern part of the basin, has led to the interpretation that the Gonjo Basin was a syncontractional basin (Studnicki-Gizbert et al., 2008). Basin structures, sedimentary facies, and varied paleocurrent directions suggested that the Gonjo Basin was fed by a proximal source (Studnicki-Gizbert et al., 2008; M. Tang et al., 2017). The strata in the Gonjo Basin are dominated by red-colored mudstones, sandstones, and rare conglomerates with a thickness of >3,000 m, reflecting predominantly alluvial fan, fan-delta, floodplain, and lacustrine deposition (Studnicki-Gizbert et al., 2008; M. Tang et al., 2017; Xizang BGMR, 1982). At the top of the sedimentary section, a few alternating layers of green carbonaceous shales, carbonates, and red mudstones are developed, suggesting a lacustrine environment (Studnicki-Gizbert et al., 2008).

A total of 542 samples along the 3,325 m magnetostratigraphic section was measured for AMS, using a KLY-3 Kappa bridge (AGICO) with an automated sample handling system and an applied field of 300 A/m at a frequency of 875 Hz. Each sample was rotated through three orthogonal planes. The AMS parameters, including $K_{1/2/3}$ (maximum/intermediate/minimum of the principle axes), Km (mean susceptibility), P_J (corrected degree of anisotropy), and T (shape factor) were calculated following the definitions in Tarling and Hrouda (1993). Generally, Km reflects the concentration of magnetic minerals, P_J quantifies the degree of anisotropy, and T reflects the shape of the susceptibility ellipsoid. $0 < T \leq 1$ indicates oblate shapes, whereas $-1 \leq T < 0$ indicates prolate shapes, and $T = 0$ corresponds to neutral shapes (Jelinek, 1981).

Previous rock magnetic studies (Li et al., 2020; M. Tang et al., 2017; Zhang et al., 2018) have confirmed that most likely detrital hematite is the dominant magnetic mineral in the sedimentary rocks of the Gonjo Basin, with a minor contribution of magnetite in some samples. To further identify the relative content of magnetite and hematite in the sediments, high field isothermal remanent magnetization (IRM) acquisition curves were analyzed based on cumulative log Gaussian analysis (Kruiver et al., 2001).

3. Results

Figure 1d shows stereonet projections of the three principle axes for all the samples before and after bedding correction. In *tilt-corrected* coordinates, the K_1 directions are generally subhorizontal and well grouped in NNW-SSE direction and generally parallel to the fold axis that deformed the basin fill; the K_3 axes are near bedding perpendicular and show a slight girdle distribution toward the SW. Such distributions of the principal anisotropy axes are inconsistent with the varied paleocurrent directions of the Gonjo Basin but instead are commonly found in folded sediments in foreland basins in general (Charreau et al., 2009; Gilder et al., 2001; Huang et al., 2006; Kodama, 1997; Li et al., 2014; Parés et al., 1999; Sagnotti et al., 1998; Soto et al., 2016; Z. Tang et al., 2012), indicating that the original sedimentary fabric was overprinted by weak tectonic-induced strain. Interestingly, the AMS fabrics and parameters show significant changes with stratigraphic position in the section (Figures 2 and 3) and are subdivided into three intervals:

Interval I (0–765 m, 69–65.4 Ma) is characterized by the largest values of P_J (ranging from 1.01–1.44, note the different scale of the X axis before and after 765 m in Figure 2c) and the mean magnetic susceptibility Km (ranging from $18–488 \times 10^{-6}$ SI) except the lowest 80 m (Figures 2b and 2c). The K_1 principal axes are distributed in NNW-SSE directions, and K_3 principal axes inclinations are almost perpendicular to the bedding plane (average: 87.6°, see supporting information Table S1 for the statistical mean direction of principle axes and AMS parameters) (Figure 3a). The AMS ellipsoid shapes defined by K_1, K_2, and K_3 are dominantly oblate with T typically >0.5 (average value: 0.6) (Figure 2d).

Interval II (765–2,154.5 m, 65.4–52 Ma) is marked by a sharp decrease of P_J (from 1.005–1.1) and Km (from $32–287 \times 10^{-6}$ SI), which subsequently show a gradual increase up section (Figures 2b and 2c). The K_1 principal axes are distributed subhorizontally in approximately N-S orientation and K_3 principal axes are mostly perpendicular to the bedding plane (average: 80.5°) (Figure 3b). However, in the lower part of this interval, the K_3 principal axes orientations are shallow and the AMS axes are randomly scattered (Figures 2e and 2f and yellow dots in Figure 3b). We suspect that this is due to the low susceptibility in these intervals, which prohibits measurement of a precise AMS direction. This is supported by much larger uncertainties of principal axes directions for specimens that have low Km (see supporting
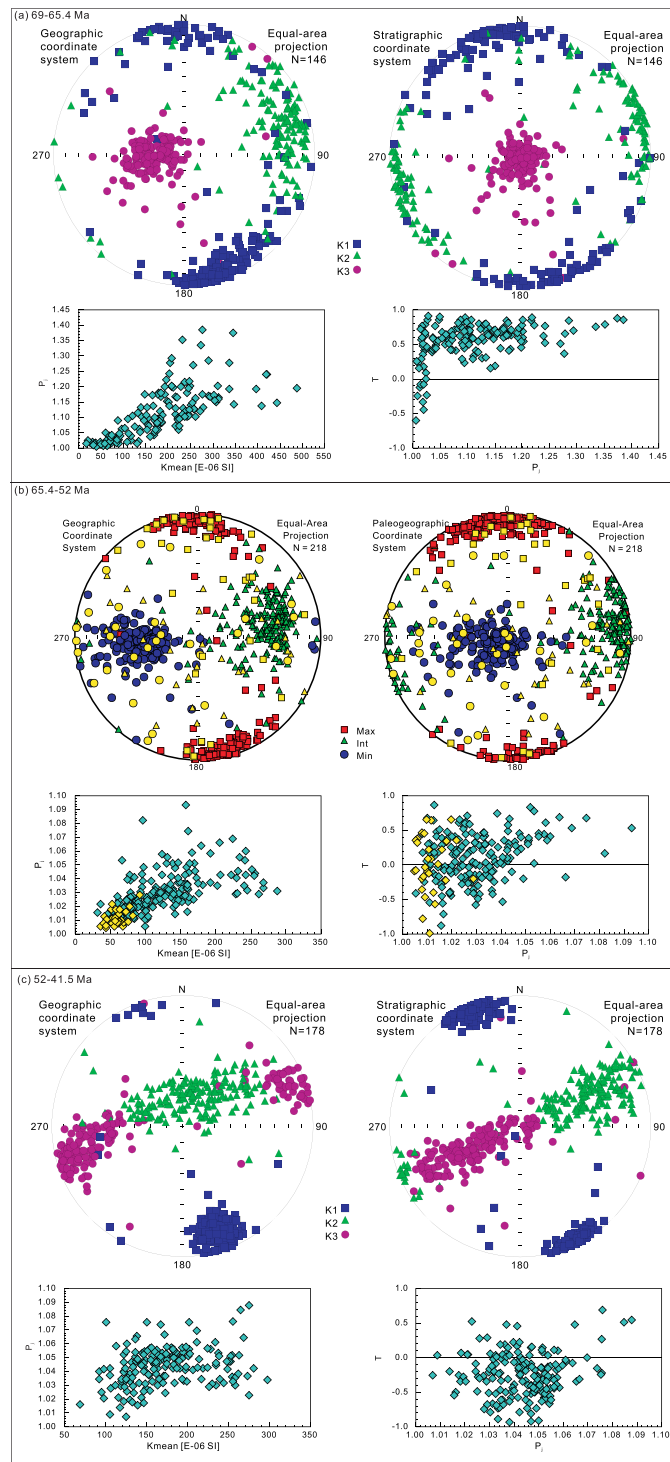
Figure 3. Equal-area projections of the three principle axes and P_J-Km of the three intervals as shown in Figure 2. (a) Interval I (0–765 m, 69–65.4 Ma), (b) Interval II (765–2,154.5 m, 65.4–52 Ma), and (c) Interval III (2,154.5–3,325 m, 52–41.5 Ma). The yellow dots in Figure 2b represent the specimens in the lower part of Interval II which have relative low magnetic susceptibility.

information Figure S1). Despite the change of magnetic susceptibility, oscillations of the shape parameter T remain fairly constant around a mean value of $T = 0.1$ in this interval (Figure 2d), suggesting a dominance of neutral shapes in Interval II.
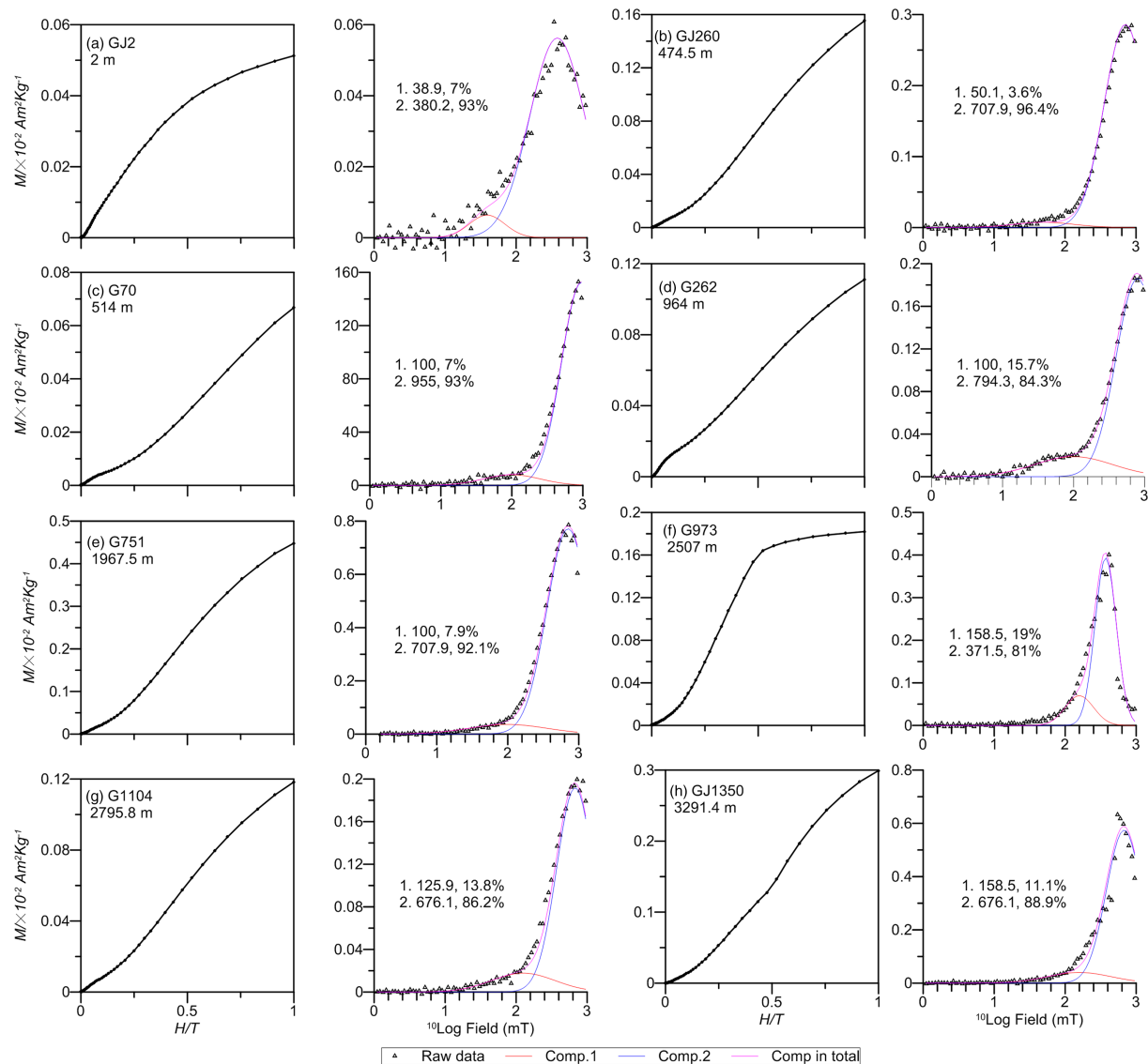
Figure 4. The isothermal remanent magnetization (IRM) acquisition curves (left) and their corresponding component analyses (right) on representative samples from the Gonjo Basin. 1 and 2 represent the low- and high-coercivity components, respectively, with $B_{1/2}$ and relative contributions to saturation IRM.

Like Interval II, P_J and Km in Interval III (2,154.5–3,325 m, 52–41.5 Ma) also increase upward in the strata (Figures 2b and 2c). P_J ranges from 1.007–1.09 and Km varies from 69–297 $\times 10^{-6}$ SI. The most prominent feature in Interval III is the change of T to negative values (mean value: −0.24) (Figure 2d), which indicates triaxial-prolate shapes of the AMS ellipsoid in this interval. This is consistent with the distribution of K_3 principal axes orientations (average: 59.5°) describing a SW-NE girdle distribution (Figure 3c), suggesting that the minimum axis parallel to the shortening direction becomes near-equal to the compaction-induced, vertical shortening (Figure 2c). Notably, the grouping of K_1 principal axes in Interval III is significantly tighter than in Intervals I and II (Figure 3c).

The IRM component analyses identified two components in all the samples (Figure 4): a minor low-coercivity component and a pronounced high-coercivity component. For the low-coercivity component, most samples have $B_{1/2}$ (the field at which half of the saturation IRM is reached) larger than 100 mT, which could be maghemite or fine-grained (pigmentary) hematite. The two samples from Interval I have $B_{1/2}$ less than 50 mT (Figures 4a and 4b), which is a reasonable value for magnetite. The high-coercivity component of all samples has $B_{1/2}$ between ~350 and 900 mT, which is consistent with the magnetic properties of hematite.

4. Discussion

4.1. Source of the Magnetic Susceptibility

Magnetic susceptibility of rocks contains contributions from diamagnetic, paramagnetic matrix minerals, ferrimagnetic, and antiferromagnetic minerals. AMS residing in magnetite reflects a preferred grain shape orientation, whereas AMS due to hematite or paramagnetic minerals reflects preferred crystallographic orientation (Borradaile & Henry, 1997; Parés et al., 1999), which is controlled by tectonic strain. Therefore, it is essential to identify which mineral(s) dominate(s) the AMS when applying AMS data to tectonics. As the volume susceptibility of magnetite (~1 SI, Tauxe, 2010) is ~1,000 times greater than most minerals (Gilder et al., 2001; Parés, 2004), magnetite will dominate the magnetic behavior of sediments if magnetite content exceeds 0.5% of the iron oxide. The mean magnetic susceptibility (Km) of Gonjo sediments, however, varies from 18–488×10^{-6} SI with a mean value of 155×10^{-6} SI. The overall very weak values of bulk susceptibility argue against a significant contribution from magnetite and suggest that the susceptibility, and hence, the AMS are dominated by antiferromagnetic (e.g., hematite) and paramagnetic minerals. This is consistent with our IRM component analysis results, suggesting that hematite can be interpreted as the dominant magnetic mineral in the sedimentary sequence of the Gonjo Basin, with a minor contribution from magnetite only at the bottom of the section, as evidenced by the minor low-coercivity component with coercivity peaks of 38.9 and 50.1 mT (Figures 4a and 4b).

As shown in Figure 1d, P_J exhibits a very weak correlation to the Km, suggesting that magnetic minerals concentration may partly control P_J. However, our results show that T is independent of Km, and both P_j and T are independent of lithology. Therefore, the AMS of the Gonjo Basin recorded a crystallographic preferred orientation of hematite and paramagnetic minerals aligned by tectonic strain. The clustering of K_3 principal axes inclinations to near vertical after bedding correction indicates that the magnetic fabrics were acquired before the tilting of the sedimentary sequences, that is, during or shortly after deposition during incipient deformation and diagenesis and mainly related to layer-parallel shortening (Larrasoana et al., 2004; Parés, 2004; Parés et al., 1999; Soto et al., 2009). This is further supported by the coincident change between AMS K_1 principal axes orientations and paleomagnetic declinations: both indicate a slight counterclockwise rotation at 69–67 Ma, no significant rotation from 67–52 Ma, a clockwise rotation at 52–48 Ma, followed by no significant rotation between 48 and 41.5 Ma (Figures 2f and 2g). This interesting result, as also observed in the Subei Basin of northeast Tibet (Gilder et al., 2001), suggests that the AMS results of the Gonjo Basin are robust recorders of tectonic strain and changes therein during the sediments' deposition.

4.2. Relationship Between AMS and Strain

AMS can be geometrically described by an ellipsoid, which is qualitatively related to the finite strain state. Ramsay and Huber (1983) developed the classical relationship between strain magnitude and cleavage intensity in sediments, where the latter can be described by the magnetic fabric. Six main stages of fabric development have been distinguished with increasing strain: undeformed condition, earliest deformation, pencil structure, weak cleavage, strong cleavage, and stretching lineation (Parés, 2004). We will briefly describe the first four stages before obvious cleavage can be observed at outcrop scale.

An "undeformed condition" of a sedimentary fabric is characterized by parallelism of the magnetic foliation and the bedding plane, with a relatively low degree of anisotropy and an oblate shape of the AMS ellipsoid. The K_1 and K_2 axes are disorderly scattered within a plane parallel to bedding, whereas the K_3 axes are vertical to the bedding plane. In the case whereby the sediments are transported by wind or water, and the AMS resides in magnetic particles that carry shape anisotropy, for example, magnetite, a weak magnetic lineation may have formed by alignment of minerals which can be reflected by K_1 (e.g., R. Zhu et al., 2004), either parallel or normal to the wind/paleocurrent direction, depending on the hydrodynamic condition (Tauxe, 2010). After minor layer-parallel shortening, an "earliest deformation" stage is formed, which is characterized by grouping of K_1 to develop magnetic lineation that is perpendicular to the shortening direction and parallel to the tensile direction. The magnetic foliation is still parallel to the bedding plane and K_3 axes are normal to the magnetic foliation. As shortening increases, the clustering of K_1 and K_2 continues to increase. An intersection lineation by definition implies canting of particles and therefore a small elongation of K3 principal axes in the direction of the compression, forming a girdle with K_2 that is parallel to the principal strain axis. The AMS ellipsoid changes from oblate to prolate to form a "pencil structure" fabric (e.g.,

Maffione et al., 2015; Parés et al., 1999). Further increasing strain leads to the production of a weak or incipient cleavage that crosscuts bedding, corresponding to a "weak cleavage" fabric. The K_3 distribution gradually changes from girdle to cluster parallel to both the bedding plane and shortening direction, whereas the magnetic ellipsoid remains prolate.

4.3. A Shortening Pulse of Tibet at ~52 Ma

Our AMS results between 69 and 65.4 Ma display an oblate ellipsoid with K_3 normal to bedding plane and K_1 subhorizontal and gathered around a NNW-SSE direction. This distribution is consistent with an original sedimentary fabric overprinted by a subtle NE-SW shortening, representing the earliest deformation stage. The AMS changes from oblate to neutral shape at 65.4 Ma concomitantly to a significant decrease of P_J and Km. We interpret that the AMS between 65.4 and 52 Ma represents a transition between the earliest deformation and the pencil structure that appears in 52 Ma and younger sediments, where the AMS is characterized by prolate magnetic ellipsoids, and the K_1 are tightly clustered in a NNW-SSE, fold axis-parallel orientation (Figure 3c), and the K_3 are significantly shallowed (Figure 2e) and distributed along a moderate girdle with K_2 (Figure 3c). This is consistent with the pencil structure stage, implying a significant increase in synsedimentary shortening strain and therefore tectonic deformation during this interval. This deformation may result in the ~30° rotation of the Gonjo Basin since 52 Ma, as evidenced by both the AMS K_1 principal axes orientations and paleomagnetic declinations (Figures 2f and 2g). Moreover, our results suggest that P_J is more sensitive to magnetic content, whereas T is more related to strain change, and therefore, T is a more reliable parameter to provide information regarding tectonic deformation.

The magnetostratigraphic age model for the Gonjo Basin (Figure 2i Li et al., 2020) shows that the sedimentation rate in the Gonjo Basin increased from ~8 to ~20 cm/kyr at ~52 Ma (Figure 2h). Our AMS results confirm the prediction of Li et al. (2020) that the sedimentation rate increase coincides with a sudden increase in tectonic shortening strain at 52 Ma and therefore reflects a tectonic origin rather than climate change.

Tectonic deformation of the Tibetan Plateau at ~52 Ma has been identified in previous studies. In north and northeast Tibet, a series of Cenozoic sedimentary basins were developed as a result of this deformation, for example, Qaidam, Xining, and Lanzhou Basins (Figure 1a). The Cenozoic strata unconformably overlie pre-Cenozoic strata and are dominated by conglomerates and coarse sandstones at the base. The initial age of these basins has been magnetostratigraphically constrained at ~52–54 Ma (Dai et al., 2006; Fang et al., 2019; Ji et al., 2017; Yue et al., 2001). In the central part of Tibet, a magnetostratigraphic study of Hoh Xil Basin indicates a rapid increase of sedimentation rate at ~54 Ma (Jin et al., 2018). Low-temperature thermochronology studies indicate that the Altyn Tagh and the southern Qilian Shan-Nan Shan faults initiated at ~50 Ma (Cheng et al., 2015; Jolivet et al., 2001; Yin et al., 2002), the West Qinling fault began thrusting at ~50 Ma (Clark et al., 2010), and southern and central Tibet experienced rapid exhumation around ~55–48 Ma (Hetzel et al., 2011; Jian et al., 2018; Staisch et al., 2014). Furthermore, paleomagnetic results indicate that northeast (Dupont-Nivet et al., 2004), east (Li et al., 2020), and southeast (Li et al., 2017) Tibet underwent clockwise rotation starting at ~50 Ma. These estimates rely on different types of data sets, each with their own uncertainty. The integrated high-resolution magnetostratigraphy of the Gonjo Basin providing detailed age control (Li et al. (2020) and now coupled with the extensive AMS analysis provided in this paper firmly confirms that many of these features result from a sudden increase in shortening strain starting at ~52 Ma.

4.4. Application of AMS to Decipher Long-Term Shortening History

The onset of India-Asia collision, although highly controversial, has been recently constrained at 59 ± 1 Ma, when the first Asian sediments were deposited in the Tethyan Himalayan stratigraphy that marks the northernmost continental crust on the Indian plate (Hu et al., 2015). The AMS ellipsoid shape and parameters from the Gonjo Basin, however, do not reveal a significant change at this inferred time of collision (Figures 2b–2f), which is in line with the absence of a regional change in sedimentation rate and paleomagnetic declinations from the Gonjo Basin (Figure 2; Li et al., 2020). Instead, significant upper crustal shortening of eastern Tibet at ~52 Ma, as observed by our AMS coincide with the increase of sedimentation rates and clockwise rotation of the Gonjo Basin (Li et al., 2020), and the sudden drop of India-Asia convergence rate from ~160 to ~80 mm/yr starting around 52 Ma (Copley et al., 2010; van Hinsbergen et al., 2011). All these

lines of evidence suggest that, although the India-Asia initial collision began at 59 ± 1 Ma, significant tectonic deformation in Tibet and slowdown of India did not occur until 52 Ma.

Given its setting, shortening of the Tibetan Plateau has long been interpreted as a direct result of collision of India with Asia (e.g., Patriat & Achache, 1984), and the mismatch between onset of collision and upper crustal shortening increase may be surprising. This may suggest that the sedimentary record in the Tethyan Himalaya reflects either collision of a far-traveled Asia-derived arc remnant with the northern Indian margin, rather than with Asia (e.g., Kapp & DeCelles, 2019), or collision of an extended continent of Tethyan Himalaya from India with Asia (van Hinsbergen et al., 2012). On the other hand, comparison with other modern orogens shows that there is no systematic relationship between upper crustal shortening and collision. For instance, the Andean orogen formed due to upper crustal shortening during oceanic subduction (e.g., Oncken et al., 2006), whereas long-lived continental subduction in the Mediterranean region has for 100 Myr or more been associated with generally no upper plate shortening, or even widespread upper crust extension instead of shortening (van Hinsbergen et al., 2020). It has long been shown that significant "Andean-style" orogenesis occurred in Tibet well before initial collision with India (e.g., Kapp & DeCelles, 2019, and references therein). Our results suggest that also the Cenozoic shortening and by inference uplift of the Tibetan Plateau may not be directly tied to the nature of the lithosphere consumed at the south Tibetan plate boundary.

The slowdown of India at ~52 Ma may reflect deeper-seated processes related to the interaction of the subducting Indian lithosphere with the mantle (van Hinsbergen et al., 2019; D. Zhu et al., 2015). However, regardless of the geodynamic causes underpinning the India-Asia plate motion changes or the 52 Ma shortening pulse in Tibet, the analysis of geodynamic causes of upper crustal deformation require tight age constraints between collisional, plate kinematic, and climatic processes. Our analysis shows that integrated paleomagnetic and magnetic fabric data sets can provide such tight age constraints that may lie at the basis for further analysis of the geodynamic and climatic processes that shape the Earth's crust and surface.

5. Conclusions

In this study, we present AMS results from the Gonjo Basin of 69–41.5 Ma, which provide information regarding the strain change and tectonic deformation of eastern Tibet during the India-Asia collision. The AMS results suggest that the Gonjo Basin was under approximately NNE-SSW direction shortening persistently from 69–41.5 Ma, consistent with the previously interpreted syncontractional nature of the basin. Our AMS results provide independent evidence that the increase of sedimentation rates in the Gonjo Basin at 52 Ma as indicated by previous magnetostratigraphic analysis reflects a tectonic pulse and that there was no such pulse upon initial continental collision recorded in the Tethyan Himalaya at 59 ± 1 Ma. From this we infer that upper crustal shortening may not directly reflect the change in nature of the subducting lithosphere and can thus not be used to date collision. Our results illustrate that the deciphering of geodynamic, or climatic, influence on plateau formation and plateau rise and vice versa require independent, high-resolution dating of upper crustal shortening, and that integrated paleomagnetic research may provide such dating.

References

Borradaile, G., & Henry, B. (1997). Tectonic applications of magnetic susceptibility and its anisotropy. *Earth Science Reviews*, *42*(1), 49–93. https://doi.org/10.1016/S0012-8252(96)00044-X

Borradaile, G. J. (1988). Magnetic susceptibility, petrofabrics and strain. *Tectonophysics*, *156*(1–2), 1–20. https://doi.org/10.1016/0040-1951(88)90279-X

Charreau, J., Chen, Y., Gilder, S., Barrier, L., Dominguez, S., Augier, R., et al. (2009). Neogene uplift of the Tian Shan Mountains observed in the magnetic record of the Jingou River section (northwest China). *Tectonics*, *28*, TC2008. https://doi.org/10.1029/2007tc002137

Cheng, F., Guo, Z., Jenkins, H. S., Fu, S., & Cheng, X. (2015). Initial rupture and displacement on the Altyn Tagh fault, northern Tibetan Plateau: Constraints based on residual Mesozoic to Cenozoic strata in the western Qaidam Basin. *Geosphere*, *11*(3), 921–942. https://doi.org/10.1130/ges01070.1

Clark, M. K., Farley, K. A., Zheng, D., Wang, Z., & Duvall, A. R. (2010). Early Cenozoic faulting of the northern Tibetan Plateau margin from apatite (U–Th)/He ages. *Earth and Planetary Science Letters*, *296*(1), 78–88. https://doi.org/10.1016/j.epsl.2010.04.051

Copley, A., Avouac, J. P., & Royer, J. Y. (2010). India-Asia collision and the Cenozoic slowdown of the Indian plate: Implications for the forces driving plate motions. *Journal of Geophysical Research*, *115*, B03410. https://doi.org/10.1029/2009JB006634

Dai, S., Fang, X. M., Dupont-Nivet, G., Song, C. H., Gao, J. P., Krijgsman, W., et al. (2006). Magnetostratigraphy of Cenozoic sediments from the Xining Basin: Tectonic implications for the northeastern Tibetan Plateau. *Journal of Geophysical Research*, *111*, B11102. https://doi.org/10.1029/2005jb004187

Dupont-Nivet, G., Horton, B. K., Butler, R. F., Wang, J., Zhou, J., & Waanders, G. L. (2004). Paleogene clockwise tectonic rotation of the Xining-Lanzhou region, northeastern Tibetan Plateau. *Journal of Geophysical Research*, *109*, B04401. https://doi.org/10.1029/2003jb002620

Fang, X., Fang, Y., Zan, J., Zhang, W., Song, C., Appel, E., et al. (2019). Cenozoic magnetostratigraphy of the Xining Basin, NE Tibetan Plateau, and its constraints on paleontological, sedimentological and tectonomorphological evolution. *Earth Science Reviews*, *190*, 460–485. https://doi.org/10.1016/j.earscirev.2019.01.021

Gilder, S., Chen, Y., & Sen, S. (2001). Oligo-Miocene magnetostratigraphy and rock magnetism of the Xishuigou section, Subei (Gansu Province, western China) and implications for shallow inclinations in central Asia. *Journal of Geophysical Research*, *106*(12), 30,505–30,522. https://doi.org/10.1029/2001JB000325

Gong, Z., van Hinsbergen, D. J. J., Vissers, R. L. M., & Dekkers, M. J. (2009). Early cretaceous syn-rotational extension in the Organyà basin—New constraints on the palinspastic position of Iberia during its rotation. *Tectonophysics*, *473*, 312–323. https://doi.org/10.1016/j.tecto.2009.03.003

Graham, J. (1954). Magnetic susceptibility anisotropy, an unexploited petrofabric element. *Geological Society of America Bulletin*, *65*, 1257–1258.

Guo, Z., Ruddiman, W. F., Hao, Q., Wu, H., Qiao, Y., Zhu, R. X., et al. (2002). Onset of Asian desertification by 22 Myr ago inferred from loess deposits in China. *Nature*, *416*(6877), 159–163. https://doi.org/10.1038/416159a

Hetzel, R., Dunkl, I., Haider, V., Strobl, M., von Eynatten, H., Ding, L., & Frei, D. (2011). Peneplain formation in southern Tibet predates the India-Asia collision and plateau uplift. *Geology*, *39*(10), 983–986. https://doi.org/10.1130/G32069

Hu, X., Garzanti, E., Moore, T., & Raffi, I. (2015). Direct stratigraphic dating of India-Asia collision onset at the Selandian (middle Paleocene, 59 ± 1 Ma). *Geology*, *43*(10), 859–862. https://doi.org/10.1130/g36872.1

Huang, B., Piper, J., Peng, S., Liu, T., Li, Z., Wang, Q., & Zhu, R. (2006). Magnetostratigraphic study of the Kuche Depression, Tarim Basin, and Cenozoic uplift of the Tian Shan Range, Western China. *Earth and Planetary Science Letters*, *251*(3–4), 346–364. https://doi.org/10.1016/j.epsl.2006.09.020

Jelinek, V. (1981). Characterization of the magnetic fabric of rocks. *Tectonophysics*, *79*(3–4), T63–T67.

Ji, J., Zhang, K., Clift, P. D., Zhuang, G., Song, B., Ke, X., & Xu, Y. (2017). High-resolution magnetostratigraphic study of the Paleogene-Neogene strata in the Northern Qaidam Basin: Implications for the growth of the Northeastern Tibetan Plateau. *Gondwana Research*, *46*, 141–155. https://doi.org/10.1016/j.gr.2017.02.015

Jian, X., Guan, P., Zhang, W., Liang, H., Feng, F., & Fu, L. (2018). Late Cretaceous to early Eocene deformation in the northern Tibetan Plateau: Detrital apatite fission track evidence from northern Qaidam basin. *Gondwana Research*, *60*, 94–104. https://doi.org/10.1016/j.gr.2018.04.007

Jin, C., et al. (2018). Magnetostratigraphy of the Fenghuoshan Group in the Hoh Xil Basin and its tectonic implications for India–Eurasia collision and Tibetan Plateau deformation. *Earth and Planetary Science Letters*, *486*, 41–53. https://doi.org/10.1016/j.epsl.2018.01.010

Jolivet, M., Brunel, M., Seward, D., Xu, Z., Yang, J., Roger, F., et al. (2001). Mesozoic and Cenozoic tectonics of the northern edge of the Tibetan Plateau: Fission-track constraints. *Tectonophysics*, *343*(1–2), 111–134. https://doi.org/10.1016/S0040-1951(01)00196-2

Kapp, P., & DeCelles, P. (2019). Mesozoic-Cenozoic geological evolution the Himalayan-Tibetan orogen and working tectonic hypothese. *American Journal of Science*, *319*, 159–254. https://doi.org/10.2475/03.2019.01

Kissel, C., Barrier, E., Laj, C., & Lee, T. Q. (1986). Magnetic fabric in "undeformed" marine clays from compressional zones. *Tectonics*, *5*, 769–781. https://doi.org/10.1029/TC005i005p00769

Kodama, K. P. (1997). A successful rock magnetic technique for correcting paleomagnetic inclination shallowing: Case study of the Nacimiento Formation, New Mexico. *Journal of Geophysical Research*, *102*(B3), 5193–5205. https://doi.org/10.1029/96JB03833

Kruiver, P., Dekkers, M. J., & Heslop, D. (2001). Quantification of magnetic coercivity components by the analysis of acquisition curves of isothermal remanent magnetisation. *Earth and Planetary Science Letters*, *189*(3), 269–276. https://doi.org/10.1016/S0012-821X(01)00367-3

Larrasoana, J., Pueyo, E. L., & Parés, J. M. (2004). *An integrated AMS, structural, palaeo-and rock-magnetic study of Eocene marine marls from the Jaca-Pamplona basin (Pyrenees, N Spain); new insights into the timing of magnetic fabric acquisition in weakly deformed mudrocks*, (pp. 127–143). London: Geological Society, London, Special Publications. https://doi.org/10.1144/GSL.SP.2004.238.01.10

Li, S., van Hinsbergen, D. J. J., Najman, Y., Jing, L.-Z., Deng, C., & Zhu, R. (2020). Does pulsed Tibetan deformation correlate with Indian plate motion changes? *Earth and Planetary Science Letters*, *536*, 116,144. https://doi.org/10.1016/j.epsl.2020.116144

Li, S. H., Advokaat, E. L., van Hinsbergen, D. J. J., Koymans, M., Deng, C., & Zhu, R. (2017). Paleomagnetic constraints on the Mesozoic-Cenozoic paleolatitudinal and rotational history of Indochina and South China: Review and updated kinematic reconstruction. *Earth Science Reviews*, *171*, 58–77. https://doi.org/10.1016/j.earscirev.2017.05.007

Li, S. H., Deng, C. L., Greig, P., Yao, H. T., Huang, S., Liu, C. Y., et al. (2014). Tectonic and sedimentary evolution of the late Miocene–Pleistocene Dali Basin in the southeast margin of the Tibetan Plateau: Evidences from anisotropy of magnetic susceptibility and rock magnetic data. *Tectonophysics*, *629*, 362–377. https://doi.org/10.1016/j.tecto.2014.05.035

Maffione, M., Hernandez-Moreno, C., Ghiglione, M. C., Speranza, F., van Hinsbergen, D. J. J., & Lodolo, E. (2015). Constraints on deformation of the Southern Andes since the cretaceous from anisotropy of magnetic susceptibility. *Tectonophysics*, *665*, 236–250. https://doi.org/10.1016/j.tecto.2015.10.008

Mattei, M., Sagnotti, L., Faccenna, C., & Funiciello, R. (1997). Magnetic fabric of weakly deformed clay-rich sediments in the Italian peninsula: Relationship with compressional and extensional tectonics. *Tectonophysics*, *271*(1), 107–122. https://doi.org/10.1016/S0040-1951(96)00244-2

Molnar, P. (2004). Late Cenozoic increase in accumulation rates of terrestrial sediment: How might climate change have affected erosion rates? *Annual Review of Earth and Planetary Sciences*, *32*, 67–89. https://doi.org/10.1146/annurev.earth.32.091003.143456

Molnar, P., & Stock, J. M. (2009). Slowing of India's convergence with Eurasia since 20 Ma and its implications for Tibetan mantle dynamics. *Tectonics*, *28*, TC3001. https://doi.org/10.1029/2008tc002271

Oncken, O., Hindle, D., Kley, J., Elger, K., Victor, P., & Schemmann, K. (2006). *Deformation of the central Andean upper crustal system—Facts, fiction, and constraints for plateau models, The Andes*, (pp. 3–27). Berlin, Heidelberg: Springer.

Parés, J. (2004). How deformed are weakly deformed mudrocks? Insights from magnetic anisotropy. In F. Martín-Hernández, C. M. Lüneburg, C. Aubourg, & M. Jackson (Eds.), *Magnetic fabric: Methods and applications*, (pp. 191–203). London: Geological society, London, special publications. https://doi.org/10.1144/GSL.SP.2004.238.01.13

Parés, J., van der Pluijm, B. A., & Dinarès-Turell, J. (1999). Evolution of magnetic fabrics during incipient deformation of mudrocks (Pyrenees, northern Spain). *Tectonophysics*, *307*(1), 1–14. https://doi.org/10.1016/S0040-1951(99)00115-8

Patriat, P., & Achache, J. (1984). India–Eurasia collision chronology has implications for crustal shortening and driving mechanism of plates. *Nature*, *311*, 615–621. https://doi.org/10.1038/311615a0

Ramsay, J. G., & Huber, M. I. (1983).*The Techniques of Modern Structural Geology, 1. Strain Analysis* (p. 307). London: Academic Press.

Sagnotti, L., Speranza, F., Winkler, A., Mattei, M., & Funiciello, R. (1998). Magnetic fabric of clay sediments from the external northern Apennines (Italy). *Physics of the Earth and Planetary Interiors*, *105*(1), 73–93. https://doi.org/10.1016/S0031-9201(97)00071-X

Soto, R., Larrasoaña, J. C., Arlegui, L. E., Beamud, E., Oliva-Urcia, B., & Simón, J. L. (2009). Reliability of magnetic fabric of weakly deformed mudrocks as a palaeostress indicator in compressive settings. *Journal of Structural Geology*, *31*(5), 512–522. https://doi.org/10.1016/j.jsg.2009.03.006

Soto, R., Larrasoaña, J. C., Beamud, E., & Garcés, M. (2016). Early–Middle Miocene subtle compressional deformation in the Ebro foreland basin (northern Spain); insights from magnetic fabrics. *Comptes Rendus Geoscience*, *348*(3–4), 213–223. https://doi.org/10.1016/j.crte.2015.10.009

Staisch, L. M., Niemi, N. A., Hong, C., Clark, M. K., Rowley, D. B., & Currie, B. (2014). A Cretaceous-Eocene depositional age for the Fenghuoshan Group, Hoh Xil Basin: Implications for the tectonic evolution of the northern Tibet Plateau. *Tectonics*, *33*, 281–301. https://doi.org/10.1002/2013TC003367

Studnicki-Gizbert, C., Burchfiel, B. C., Li, Z., & Chen, Z. (2008). Early Tertiary Gonjo basin, eastern Tibet: Sedimentary and structural record of the early history of India-Asia collision. *Geosphere*, *4*(4), 713–735. https://doi.org/10.1130/GES00136.1

Tang, M., Liu-Zeng, J., Hoke, G. D., Xu, Q., Wang, W., Li, Z., et al. (2017). Paleoelevation reconstruction of the Paleocene-Eocene Gonjo basin, SE-central Tibet. *Tectonophysics*, *712-713*, 170–181. https://doi.org/10.1016/j.tecto.2017.05.018

Tang, Z., Huang, B., Dong, X., Ji, J., & Ding, Z. (2012). Anisotropy of magnetic susceptibility of the Jingou River section: Implications for late Cenozoic uplift of the Tian Shan. *Geochemistry Geophysics Geosystems*, *13*, Q03022. https://doi.org/10.1029/2011GC003966

Tarling, D., & Hrouda, F. (1993). *The magnetic anisotropy of rocks*, (p. 217). London: Champan and Hall.

Tauxe, L. (2010). *Essentials of Paleomagnetism*, (p. 512). Berkeley: University of California Press.

van Hinsbergen, D. J. J., Lippert, P. C., Dupont-Nivet, G., McQuarrie, N., Doubrovine, P. V., Spakman, W., & Torsvik, T. H. (2012). Greater India Basin hypothesis and a two-stage Cenozoic collision between India and Asia. *Proceedings of the National Academy of Sciences of the United States of America*, *109*(20), 7659–7664. https://doi.org/10.1073/pnas.1117262109

van Hinsbergen, D. J. J., Lippert, P. C., Li, S., Huang, W., Advokaat, E. L., & Spakman, W. (2019). Reconstructing greater India: Paleogeographic, kinematic, and geodynamic perspectives. *Tectonophysics*, *760*, 69–94. https://doi.org/10.1016/j.tecto.2018.04.006

van Hinsbergen, D. J. J., Steinberger, B., Doubrovine, P. V., & Gassmöller, R. (2011). Acceleration and deceleration of India-Asia convergence since the cretaceous: Roles of mantle plumes and continental collision. *Journal of Geophysical Research*, *116*, B06101. https://doi.org/10.1029/2010jb008051

van Hinsbergen, D. J. J., Torsvik, T., Schmid, S. M., Matenco, L., Maffione, M., Vissers, R. L. M., et al. (2020). Orogenic architecture of the Mediterranean region and kinematic reconstruction of its tectonic evolution since the Triassic. *Gond Research*, *81*, 79–229. https://doi.org/10.1016/j.gr.2019.07.009

van Hinsbergen, D. J. J., Zachariasse, W. J., Wortel, M. J. R., & Meulenkamp, J. E. (2005). Underthrusting and exhumation: A comparison between the External Hellenides and the "hot" Cycladic and "cold" South Aegean core complexes (Greece). *Tectonics*, *24*(2), TC2011. https://doi.org/10.1029/2004TC001692

Xizang BGMR (1982). *Regional geology of Xizang (Tibet) Autonomous Region*. Geological House, Beijing: Geological Memoirs Series.

Yin, A., Rumelhart, P. E., Butler, R., Cowgill, E., Harrison, T. M., Foster, D. A., et al. (2002). Tectonic history of the Altyn Tagh fault system in northern Tibet inferred from Cenozoic sedimentation. *Geological Society of America Bulletin*, *114*(10), 1257–1295. https://doi.org/10.1130/0016-7606(2002)114<1257:THOTAT>2.0.CO;2

Yue, L. P., Heller, F., Qiu, Z. X., Zhang, L., Xie, G. P., Qiu, Z. D., & Zhang, Y. X. (2001). Magnetostratigraphy and pavleo-environmental record of Tertiary deposits of Lanzhou Basin. *Chinese Science Bulletin*, *46*(1), 770–773. https://doi.org/10.1007/BF03187220

Zhang, Y., Huang, W., Huang, B., van Hinsbergen, D. J. J., Yang, T., Dupont-Nivet, G., & Guo, Z. (2018). 53–43 Ma deformation of eastern Tibet revealed by three stages of tectonic rotation in the Gongjue basin. *Journal of Geophysical Research: Solid Earth*, *123*, 3320–3338. https://doi.org/10.1002/2018JB015443

Zhu, D. C., Wang, Q., Zhao, Z. D., Chung, S. L., Cawood, P. A., Niu, Y., et al. (2015). Magmatic record of India-Asia collision. *Scientific Reports*, *5*, 14,289. https://doi.org/10.1038/srep14289

Zhu, R., Liu, Q., & Jackson, M. J. (2004). Paleoenvironmental significance of the magnetic fabrics in Chinese loess-paleosols since the last interglacial (<130 ka). *Earth and Planetary Science Letters*, *221*(1), 55–69. https://doi.org/10.1016/S0012-821X(04)00103-7